nature physics

LETTERS

https://doi.org/10.1038/s41567-019-0698-y

Light-induced anomalous Hall effect in graphene

J. W. McIver[1,3]*, B. Schulte[1,3], F.-U. Stein[1,3], T. Matsuyama[1], G. Jotzu[1], G. Meier[1] and A. Cavalleri[1,2]*

Many non-equilibrium phenomena have been discovered or predicted in optically driven quantum solids[1]. Examples include light-induced superconductivity[2,3] and Floquet-engineered topological phases[4–8]. These are short-lived effects that should lead to measurable changes in electrical transport, which can be characterized using an ultrafast device architecture based on photoconductive switches[9]. Here, we report the observation of a light-induced anomalous Hall effect in monolayer graphene driven by a femtosecond pulse of circularly polarized light. The dependence of the effect on a gate potential used to tune the Fermi level reveals multiple features that reflect a Floquet-engineered topological band structure[4,5], similar to the band structure originally proposed by Haldane[10]. This includes an approximately 60 meV wide conductance plateau centred at the Dirac point, where a gap of equal magnitude is predicted to open. We find that when the Fermi level lies within this plateau the estimated anomalous Hall conductance saturates around $1.8 \pm 0.4\, e^2/h$.

Optical driving has been proposed as a means to engineer topological properties in topologically trivial systems[4–8]. One proposal for such a 'Floquet topological insulator' is based on breaking time-reversal symmetry in graphene through a coherent interaction with circularly polarized light[4]. In this theory, the light field drives electrons in circular trajectories through the band structure (Fig. 1a). Close to the Dirac point, these states are predicted to acquire a non-adiabatic Berry phase with each optical cycle, and the contributions are equal and opposite for the upper and lower bands. This time-averaged extra phase accumulation amounts to an energy shift that lifts the degeneracy of the Dirac point and opens a topological gap in the effective Floquet band structure (Fig. 1b).

The non-trivial topology of the Floquet bands forming this gap arises from their non-zero Berry curvature distribution[4,5], which integrated over the Brillouin zone defines a topological invariant, called the Chern number[11–14]. Topologically protected transport is predicted to develop if the Fermi level (E_F) lies inside the gap, exhibiting an anomalous Hall effect carried by edge states in the absence of an applied magnetic field[5,10–15]. This corresponds to the formation of a light-induced Chern insulator, equivalent to the phase originally proposed by Haldane[10] and distinct from topological phases induced by spin–orbit interaction[12–14,16,17]. While quantum simulation experiments have validated aspects of this proposal in synthetic physical settings[18,19], and Floquet–Bloch states have been detected in a topological insulator[20], anomalous Hall currents originating from such a photon-dressed topological band structure have not been observed in a real material.

This proposal is unique because the anomalous Hall effect arises from Berry curvature that is coherently induced by light in a material where none is present in equilibrium. This is in contrast to previous observations of photoinduced anomalous Hall effects in semiconductor quantum wells[21], monolayer transition metal dichalcogenides[22] or Weyl semimetals[23], which originate from Berry curvature intrinsic to the equilibrium band structure due to broken inversion symmetry.

Inducing and detecting anomalous Hall currents in graphene presents multiple experimental challenges. The laser electric field strength required to open an observable topological gap is estimated to be of the order of 10^7–$10^8\,\mathrm{V\,m^{-1}}$, even at mid-infrared wavelengths where the effect is enhanced[4,5,15]. Hence, to avoid material damage while still providing sufficient field strength, ultrafast laser pulses must be used. Consequently, the resulting Hall conductance changes are too short lived to be probed with conventional transport techniques.

In this work, ultrafast anomalous Hall currents were detected on-chip by using a laser-triggered photoconductive switch[9]. A schematic of our device architecture is shown in Fig. 1c. An exfoliated monolayer graphene flake was transferred onto a doped silicon wafer with an oxide layer and contacted in a four-probe Hall geometry using standard lithography procedures[24,25]. The metallic leads formed microstrip transmission lines in conjunction with the oxide layer and silicon wafer. These directed ultrafast anomalous Hall currents generated in the graphene to a photoconductive switch for detection. The switch consisted of a resistive amorphous silicon patch that bridged the main transmission line and a probing line. When excited with a visible ultrafast laser pulse, the switch became highly conductive and detected currents flowing in the main transmission line with a time resolution set by the silicon carrier lifetime (less than 1 ps). By adjusting the time delay between the graphene laser drive pulse (pump) and the switch trigger pulse (probe), the temporal profile of ultrafast anomalous Hall currents could be characterized. The amplitudes of the detected currents were determined by calibrating the photovoltaic response of the switch using a d.c. bias field, which is possible in our microstrip geometry because only the fundamental quasi-transverse electromagnetic mode propagates up to terahertz frequencies.

Graphene was driven using an approximately 500 fs laser pulse at a frequency of 46 THz (so that the photon energy $\hbar\omega \approx 191$ meV, wavelength $\approx 6.5\,\mu$m). Unless otherwise noted, a peak laser pulse fluence of $0.23\,\mathrm{mJ\,cm^{-2}}$ was used, corresponding to a peak intensity of $4.3 \times 10^{12}\,\mathrm{W\,m^{-2}}$ and peak electric field strength of $4.0 \times 10^7\,\mathrm{V\,m^{-1}}$ (in free space, for circular polarization). The pulses were focused to a spot size of roughly 80 μm (full-width at half-maximum), ensuring homogeneous illumination of the graphene flake and the contacts. A second ultrafast laser pulse centred at 520 nm was used to operate the photoconductive switch. The device was mounted in a microscopy cryostat designed for high-frequency transport measurements and cooled to a base temperature of 80 K. A global backgate formed by the silicon wafer and the oxide layer controlled E_F in the graphene flake. The graphene field-effect mobility was measured to be $\mu \approx 10{,}000\,\mathrm{cm^2\,V^{-1}\,s^{-1}}$ in the vicinity of the Dirac point. The results presented here are from a single device, and consistent results have been obtained using five different devices.

[1]Max Planck Institute for the Structure and Dynamics of Matter, Hamburg, Germany. [2]Department of Physics, Clarendon Laboratory, University of Oxford, Oxford, UK. [3]These authors contributed equally: J.W. McIver, B. Schulte, F.-U. Stein. *e-mail: james.mciver@mpsd.mpg.de; andrea.cavalleri@mpsd.mpg.de

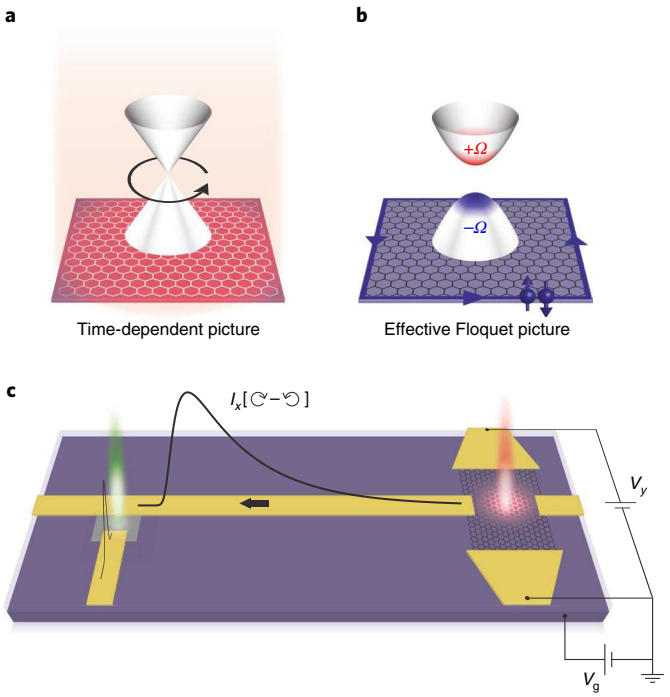

Fig. 1 | Light-induced topological Floquet bands in graphene and device architecture used to detect ultrafast anomalous Hall currents. a, A coherent interaction between graphene and circularly polarized light was predicted to open a topological band gap in the effective Floquet band dispersion[4]. **b**, The gap is characterized by the presence of Berry curvature (Ω), which is identical in the two valleys. The experimental signature of the induced non-trivial topology is the emergence of anomalous Hall currents. **c**, An exfoliated graphene monolayer with four electrical contacts (right) and a photoconductive switch for current detection (left), connected by a microstrip transmission line. The graphene was optically driven using an ultrafast mid-infrared circularly polarized laser pulse (red beam). The generated helicity-dependent $I_x[\circlearrowright-\circlearrowleft]$ were probed after a variable time delay at the photoconductive switch, which was activated by a second laser pulse (green beam). Anomalous Hall currents were measured as a function of V_y and backgate voltage V_g, the latter of which controlled the graphene E_F.

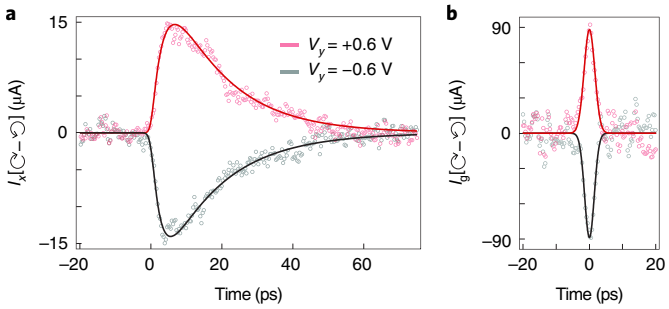

Fig. 2 | Ultrafast anomalous Hall currents in graphene driven by circularly polarized light. a, Time-resolved helicity-dependent $I_x[\circlearrowright-\circlearrowleft]$ measured at the photoconductive switch for a positive and negative V_y. The graphene Fermi level was gated to the Dirac point ($E_F=0$). Solid lines are based on the signal propagation model in Supplementary Section S3. A small background observed at $V_y=0$ was subtracted from the data sets (Supplementary Section S4). **b**, Deconvolved anomalous Hall current signals I_g accounting for the response function of the on-chip circuitry. The current amplitude has a ±22% systematic error from the calibration of the photoconductive switch. Solid lines are Gaussian fits.

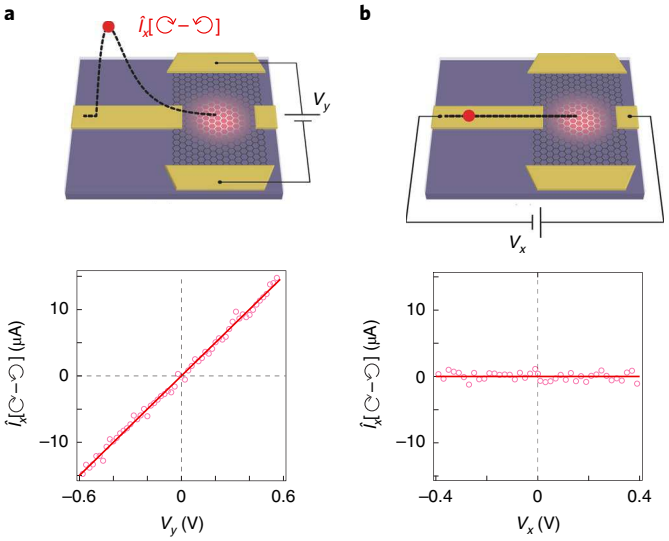

Fig. 3 | Helicity-dependent current behaviour under different source–drain voltage geometries. a,**b**, $\hat{I}_x[\circlearrowright-\circlearrowleft]$ measured as a function of V_y (**a**) and V_x (**b**). The graphene Fermi level was gated to the Dirac point ($E_F=0$). Solid lines are linear fits.

Anomalous Hall currents induced by circularly polarized light are expected to exhibit the following traits. (1) They should be generated in the transverse direction (I_x) with respect to an applied d.c. voltage bias (V_y). (2) They should reverse polarity on reversing the light helicity. (3) They should reverse polarity on reversing V_y, with a linear functional dependence. To probe (1) and (2), we directly detected the difference between currents I_x generated with right (clockwise from the perspective of the light source) versus left circular polarization (henceforth referred to as $I_x[\circlearrowright-\circlearrowleft]$), utilizing an optical polarization chopping technique.

Figure 2a displays the measured $I_x[\circlearrowright-\circlearrowleft]$ signal as a function of pump–probe time delay for a positive and negative V_y, with the Fermi level gated to the graphene Dirac point ($E_F=0$). The time-resolved signal exhibits a fast rise time followed by an exponential decay, and reverses polarity on reversing V_y. From the polarity of the signals, we determine that for right circularly polarized light propagating along $+z$ (in a right-handed coordinate system) a d.c. field applied to the graphene in the $-y$ direction induces a Hall current in the $+x$ direction.

The measured data in Fig. 2a contain a convolution between the intrinsic dynamics of anomalous Hall currents in the graphene and the response function of the circuit, which includes the contact resistance, graphene capacitance, microstrip impedance and dispersion in the transmission line. As detailed in Supplementary Section S3, we directly calibrated these system parameters to determine the deconvolved current profiles, shown in Fig. 2b. The signals have a duration of approximately 3 ps, which exceeds that of the driving laser pulse (500 fs). We believe that this difference in timescales is mainly caused by the finite size of the graphene, which leads to arrival-time differences of currents generated in different parts of the flake, as well as the sublinear dependence of the Hall current on the drive laser intensity (see below).

Having established the presence of ultrafast anomalous Hall currents in graphene, we investigated the functional dependence of $I_x[\circlearrowright-\circlearrowleft]$ on V_y at $E_F=0$. We did so by fixing the pump–probe time delay at the maximum of the $I_x[\circlearrowright-\circlearrowleft]$ signal in Fig. 2a, which we refer to as $\hat{I}_x[\circlearrowright-\circlearrowright]$, and measured the signal amplitude as a function of V_y (Fig. 3a). The data exhibit the expected linear dependence. We also investigated helicity-dependent currents generated

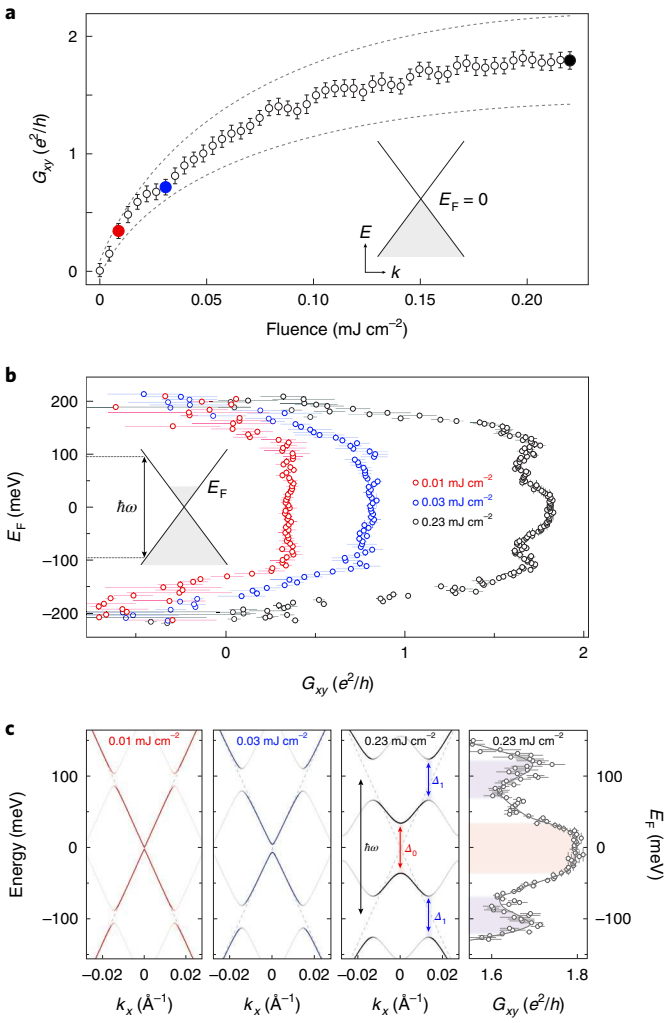

Fig. 4 | Evidence for topological Floquet bands. a, G_{xy} as a function of the peak laser drive pulse fluence. The equilibrium Fermi level was gated to the Dirac point ($E_F = 0$). Error bars are the s.e.m., and the dashed lines denote the systematic error from the calibration of the photoconductive switch. Coloured data points correspond to the fluences measured in **b**. **b**, G_{xy} as a function of the equilibrium E_F measured at three fluences. Horizontal error bars are the s.e.m. and vertical error bars denote the uncertainty related to determining the precise value of the Dirac point. The systematic error on G_{xy} is the same as in **a**. **c**, Left three panels: effective band structures for the fluences reported in **b** simulated using Floquet theory. At the highest fluence, we calculated $\Delta_0 \approx 69$ meV and $\Delta_1 \approx 56$ meV. Right panel: magnification of the high-fluence data in **b** for comparison. The solid line is the smoothed data. Shaded regions highlight the features corresponding to light-induced band gaps in the Floquet band structure.

in response to a longitudinal voltage bias V_x (Fig. 3b), which are not expected because graphene has D_{6h} point group symmetry[26]. The data in Fig. 3b confirm that no helicity-dependent longitudinal currents were generated.

We define the peak anomalous Hall conductance of the non-equilibrium state as $G_{xy} = \hat{I}_g[\circlearrowright - \circlearrowleft]/2V_y$, where $\hat{I}_g$ is the peak of the deconvolved signal in Fig. 2b. Figure 4a displays G_{xy} as a function of the laser drive pulse fluence, measured for $E_F = 0$. The data show a sublinear dependence that saturates at high fluence. At the highest achievable fluence, we estimate $G_{xy} = (1.8 \pm 0.4)\, e^2/h$, consistent with recent numerical simulations of optically driven graphene for our laser pulse parameters[27].

To characterize the predicted topological Floquet bands, we varied E_F (defined as the chemical potential without light excitation) using the backgate[28] and compared the variation in G_{xy} (Fig. 4b) with calculations of the expected effective band structures based on Floquet theory for our laser pulse parameters (Fig. 4c) (Supplementary Section S7).

We observed that for low drive fluence (red circles) G_{xy} was independent of the backgate potential for $|E_F| \lesssim 100\,\text{meV} \approx \hbar\omega/2$. In this low-excitation regime, the Floquet gap at the Dirac point (Δ_0) is too small to be observable. However, sizeable gaps Δ_1 appear precisely at $\pm\hbar\omega/2$ as a consequence of resonant Rabi splitting. Because these gaps Δ_1 are opened non-adiabatically, a non-equilibrium electron distribution can be expected in a ring of momenta surrounding the Dirac point where the photon resonance occurs, for $|E_F| \lesssim \hbar\omega/2$. We believe that the observed plateau at low fluence thus results from the resonant excitation of electrons in conjunction with the predicted Berry curvature at the Δ_1 band edges[4,15,29–33]. For $|E_F| \gtrsim \hbar\omega/2$, where first-order resonant excitations are forbidden, G_{xy} decreased to zero and eventually changed sign when approaching the dielectric breakdown threshold of the device. At higher fluences (blue and black circles), we resolved additional features near $\pm\hbar\omega/2$ in the G_{xy} versus E_F spectrum. They are closely aligned with the band edges of the calculated Δ_1, which are larger in size.

An additional feature appeared at the highest fluence (black circles): close to the Dirac point and away from the photon resonance, a conductance plateau with a width of approximately 60 meV was observed, where $G_{xy} = (1.8 \pm 0.4)\, e^2/h$ (Fig. 4c right). Remarkably, the width of this plateau is very close to the calculated width of the light-induced Δ_0 (69 meV, red shading). This suggests that at high fluence there is a second source of anomalous Hall currents carried by a distribution of electrons occupying the lower dressed band beneath Δ_0. For these momenta, the driving frequency is large compared with the splitting of the bands and a quasi-adiabatic transfer between the static and dressed bands is therefore possible. The effective Fermi level-dependent transverse transport then behaves similarly to what we would expect for gapped bands with non-zero total Berry curvature, given a Fermi–Dirac distribution, in that G_{xy} shows a plateau when E_F lies inside the band gap[11–14]. The sharpness of the decrease in G_{xy} as E_F is moved outside Δ_0 may depend on multiple factors, including the Berry curvature and non-equilibrium electron distributions in the Floquet bands, which is influenced by the frequency, amplitude and pulse-shape of the laser, as well as disorder, interactions and dissipation[4,15,29–33].

Online content

Any methods, additional references, Nature Research reporting summaries, source data, statements of code and data availability and associated accession codes are available at https://doi.org/10.1038/s41567-019-0698-y.

Received: 14 May 2019; Accepted: 19 September 2019;
Published online: 04 November 2019

References

1. Basov, D. N., Averitt, R. D. & Hsieh, D. Towards properties on demand in quantum materials. *Nat. Mater.* **16**, 1077–1088 (2017).
2. Fausti, D. et al. Light-induced superconductivity in a stripe-ordered cuprate. *Science* **331**, 189–191 (2011).
3. Mitrano, M. et al. Possible light-induced superconductivity in K_3C_{60} at high temperature. *Nature* **530**, 461–464 (2016).
4. Oka, T. & Aoki, H. Photovoltaic Hall effect in graphene. *Phys. Rev. B* **79**, 081406(R) (2009).
5. Kitagawa, T., Oka, T., Brataas, A., Fu, L. & Demler, E. Transport properties of nonequilibrium systems under the application of light: photoinduced quantum Hall insulators without Landau levels. *Phys. Rev. B* **84**, 235108 (2011).
6. Lindner, N. H., Refael, G. & Galitski, V. Floquet topological insulator in semiconductor quantum wells. *Nat. Phys.* **7**, 490–495 (2011).

7. Sie, E. et al. Valley-selective optical Stark effect in monolayer WS_2. *Nat. Mater.* **14**, 290–294 (2015).
8. Bukov, M., D'Alessio, L. & Polkovnikov, A. Universal high-frequency behavior of periodically driven systems: from dynamical stabilization to Floquet engineering. *Adv. Phys.* **64**, 139–226 (2015). 2.
9. Auston, D. H. Picosecond optoelectronic switching and gating in silicon. *Appl. Phys. Lett.* **26**, 101–103 (1975).
10. Haldane, F. D. M. Model for a quantum Hall effect without Landau levels: condensed-matter realization of the "parity anomaly". *Phys. Rev. Lett.* **61**, 2015–2018 (1988).
11. Xiao, D., Chang, M.-C. & Niu, Q. Berry phase effects on electronic properties. *Rev. Mod. Phys.* **82**, 1959–2007 (2010).
12. Hasan, M. Z. & Kane, C. L. Colloquium: Topological insulators. *Rev. Mod. Phys.* **82**, 3045–3067 (2010).
13. Qi, X.-L. & Zhang, S.-C. Topological insulators and superconductors. *Rev. Mod. Phys.* **83**, 1057–1110 (2011).
14. Bernevig, B. A. & Hughes, T. L. *Topological Insulators and Topological Superconductors* (Princeton University Press, 2013).
15. Foa Torres, L. E. F., Perez-Piskunow, P. M., Balseiro, C. A. & Usaj, G. Multiterminal conductance of a Floquet topological insulator. *Phys. Rev. Lett.* **113**, 266801 (2014).
16. Chang, C.-Z. et al. Experimental observation of the quantum anomalous Hall effect in a magnetic topological insulator. *Science* **340**, 176–170 (2013).
17. König, M. et al. Quantum spin Hall insulator state in HgTe quantum wells. *Science* **318**, 766–770 (2007).
18. Rechtsman, M. C. et al. Photonic Floquet topological insulator. *Nature* **496**, 196–200 (2013).
19. Jotzu, G. et al. Experimental realization of the topological Haldane model with ultracold fermions. *Nature* **515**, 237–240 (2014).
20. Wang, Y. H., Steinberg, H., Jarillo-Herrero, P. & Gedik, N. Observation of Floquet–Bloch states on the surface of a topological insulator. *Science* **342**, 453–457 (2013).
21. Yin, C. M. et al. Observation of the photoinduced anomalous Hall effect in GaN-based heterostructures. *Appl. Phys. Lett.* **98**, 122104 (2011).
22. Mak, K. F., McGill, K. L., Park, J. & McEuen, P. L. The valley Hall effect in MoS_2 transistors. *Science* **344**, 1489–1492 (2014).
23. Seifert, P. et al. In-plane anisotropy of the photon-helicity induced linear Hall effect in few-layer WTe_2. *Phys. Rev. B.* **99**, 161403(R) (2019).
24. Geim, A. K. & Novoselov, K. S. The rise of graphene. *Nat. Mater.* **6**, 183–191 (2007).
25. Zhang, Y., Tan, Y.-W., Stormer, H. L. & Kim, P. Experimental observation of the quantum Hall effect and Berry's phase in graphene. *Nature* **438**, 201–204 (2005).
26. Glazov, M. M. & Ganichev, S. D. High frequency electric field induced nonlinear effects in graphene. *Phys. Rep.* **535**, 101–138 (2014).
27. Sato, S. et al. Microscopic theory for the light-induced anomalous Hall effect in graphene. *Phys. Rev. B* **99**, 214302 (2019).
28. Wang, F. et al. Gate-variable optical transitions in graphene. *Science* **320**, 206–209 (2008).
29. Usaj, G., Perez-Piskunow, P. M., Foa Torres, L. E. F. & Balseiro, C. A. Irradiated graphene as a tunable Floquet topological insulator. *Phys. Rev. B* **90**, 115423 (2014).
30. Mikami, T. et al. Brillouin-Wigner theory for high-frequency expansion in periodically driven systems: application to Floquet topological insulators. *Phys. Rev. B* **93**, 144307 (2016).
31. Dehghani, H., Oka, T. & Mitra, A. Out-of-equilibrium electrons and the Hall conductance of a Floquet topological insulator. *Phys. Rev. B* **91**, 155422 (2015).
32. Sentef, M. A. et al. Theory of Floquet band formation and local pseudospin textures in pump–probe photoemission of graphene. *Nat. Commun.* **6**, 7047 (2015).
33. Morimoto, T. & Nagaosa, N. Topological nature of nonlinear optical effects in solids. *Sci. Adv.* **2**, e1501524 (2016).

Methods
All methods can be found in the Supplementary Information.

Data availability
The data represented in Figs. 2–4 are available with the online version of this paper. All other data that support the plots within this paper and other findings of this study are available from the corresponding author on reasonable request.

Acknowledgements
We acknowledge H. Aoki, L. Mathey, M. Nuske, A. Rubio, S.A. Sato, M.A. Sentef and P. Tang for fruitful discussions and B. Fiedler, B. Höhling, E. König and M. Volkmann for technical support. The research leading to these results received funding from the European Research Council under the European Union's Seventh Framework Programme (FP7/2007-2013)/ERC Grant Agreement no. 319286 (QMAC). J.W.M. received funding from the Alexander von Humboldt Foundation.

Author contributions
J.W.M. conceived the experiment together with A.C. A.C. and G.M. supervised the project. J.W.M. and F.-U.S. designed and built the experimental setup. J.W.M., F.-U.S., B.S., T.M. and G.M. developed the on-chip circuitry. B.S. fabricated the graphene devices. B.S., J.W.M. and F.-U.S. performed the measurements. B.S. and J.W.M. analysed the data with support from T.M., G.J. and G.M. Custom measurement electronics and circuit simulations were provided by T.M. and G.M. Floquet calculations were performed by G.J. The manuscript was written by J.W.M., G.J. and A.C. with contributions from all other authors.

Competing interests
The authors declare no competing interests.

Additional information
Supplementary information is available for this paper at https://doi.org/10.1038/s41567-019-0698-y.

Correspondence and requests for materials should be addressed to J.W.M. or A.C.

Reprints and permissions information is available at www.nature.com/reprints.